Journal of Catalysis 311 (2014) 458–468

Contents lists available at ScienceDirect

Journal of Catalysis

journal homepage: www.elsevier.com/locate/jcat

Hydrothermal synthesis of LTA-encapsulated metal clusters and consequences for catalyst stability, reactivity, and selectivity

Zhijie Wu [1], Sarika Goel, Minkee Choi [2], Enrique Iglesia *

Department of Chemical & Biomolecular Engineering, University of California at Berkeley, Berkeley, CA 94720, USA

ARTICLE INFO

Article history:
Received 15 October 2013
Revised 23 December 2013
Accepted 31 December 2013

Keywords:
Encapsulation
LTA zeolite
Noble metal
Hydrothermal synthesis
Oxidative dehydrogenation
Hydrogenation
Sulfur-tolerant catalyst

ABSTRACT

Noble metal clusters (Pt, Pd, Rh, Ir, Re, and Ag) are selectively encapsulated within LTA voids via hydrothermal synthesis using metal precursors with ligands (NH_3 for Pt and Ir; ethylenediamine for Pd, Rh, Re and Ag) that prevent their premature precipitation as colloidal oxyhydroxides. Such stability appears to be necessary and sufficient for successful encapsulation of cationic precursors during nucleation and growth of zeolite frameworks. Mean cluster diameters measured by titration of exposed metal atoms (H_2 on Pt, Pd, Rh, Ir and Re; O_2 on Ag; 1.1–1.8 nm) and by transmission electron microscopy (1.2–1.9 nm) were similar, indicating that cluster surfaces were clean and accessible to molecules used as titrants or reactants. Metal clusters were narrowly distributed in size and stable against sintering and coalescence during oxidative thermal treatments (573–873 K). Encapsulation selectivities were measured from turnover rates for reactions of small and large reactants, specifically hydrogenation of alkenes (ethene and isobutene) and oxidation of alkanols (methanol, ethanol, and isobutanol), which reflect the restricted access to encapsulated clusters by the larger molecules. These encapsulation selectivities, which reflect the ratio of metal surface areas within and outside LTA crystals ranged from 7.5 to 83 for all samples. Confinement within LTA crystals protects clusters from contact with thiophene and allows ethene hydrogenation to proceed at thiophene concentrations that fully suppressed reactivity for metal clusters dispersed on mesoporous SiO_2. These protocols provide a general strategy for encapsulating clusters within small-pore zeolite voids, for which post-synthesis exchange is infeasible. Their successful encapsulation protects such clusters from coalescence and growth and allows them to select reactants and reject poisons based on their molecular size.

1. Introduction

The encapsulation of metal or oxide clusters within small-pore zeolites provides potential routes to prepare catalysts with small metal clusters uniform in size, to select reactants, transition states and products based on molecular size, and to protect such clusters against sintering or poisoning during thermal treatment or catalysis [1–4]. Such strategies, however, present formidable synthetic and characterization challenges. Encapsulation within small-pore (8-membered ring (8-MR)) and medium-pore (10-MR) zeolites cannot be achieved through post-synthesis exchange, impregnation [5], or adsorption/decomposition of metal complexes, because multivalent cations in aqueous media form solvated oligomeric complexes larger than the small apertures provided by the windows in these zeolites [2,3,6]. Therefore, metal precursors must be present during hydrothermal synthesis and must remain stable at the demanding conditions required for hydrothermal crystallization of aluminosilicate gels into zeolite frameworks with pores of small (0.3–0.5 nm) or medium (0.5–0.6 nm) size [6–27].

The successful encapsulation of Pt clusters within LTA [6–14] and MFI [15], of Ru clusters within LTA [16] and MFI [17], of Rh clusters within LTA [18–22], and of Au clusters within MFI [23] have been reported via hydrothermal syntheses. These studies recognized the need for metal precursors to be present during zeolite crystallization and inferred the success of encapsulation from chemisorption uptakes or transmission electron micrographs. These reports of successful encapsulation, however, used metal precursors that precipitate as colloidal oxyhydroxides at the pH and temperatures required for zeolite synthesis [24–29], making the reported encapsulations infeasible.

Here, we report a general strategy for the encapsulation of metal and oxide clusters within LTA by choosing ligands that stabilize metal cations and protect the cationic moieties against precipitation as colloidal oxyhydroxides during hydrothermal synthesis of zeolites (Scheme 1) (Table 1, solution behavior of various metal complexes at hydrothermal synthesis conditions in the absence of SiO_2). Avoiding premature precipitation allows zeolite building

* Corresponding author. Fax: +1 (510) 642 4778.
E-mail address: iglesia@berkeley.edu (E. Iglesia).
[1] Current address: State Key Laboratory of Heavy Oil Processing and the Key Laboratory of Catalysis of CNPC, China University of Petroleum, Beijing 102249, China.
[2] Current address: Department of Chemical and Biomolecular Engineering, KAIST, 291 Daehak-ro, Yuseong-gu, Daejeon 305-701, Republic of Korea.

0021-9517/$ - see front matter © 2014 Elsevier Inc. All rights reserved.
http://dx.doi.org/10.1016/j.jcat.2013.12.021

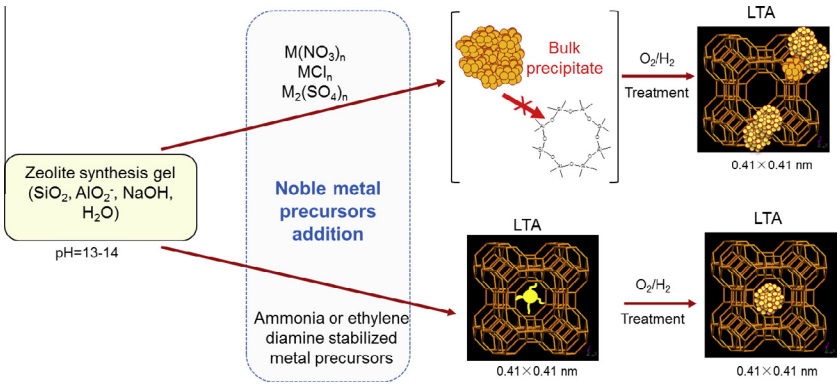

Scheme 1. Schematic of the process for encapsulation of metal clusters within LTA voids.

Table 1
Solubility product constants (K_{sp}) of metal hydroxides and solubility quotients (Q_c) of metal cations and hydroxide ions and solution behavior of various metal complexes at hydrothermal synthesis conditions in the absence of SiO_2.

Metal	Precursors (10^{-2} mol/L)	Solubility product constant (K_{sp}) of hydroxides at 298 K[a]	Solubility quotient (Q_c) at 298 K[b]	Behavior at zeolite synthesis conditions (in the absence of SiO_2)[c]
Pt	$Pt(NO_3)_2$	1.0×10^{-35}, $Pt(OH)_2$	1.5×10^{-5}	X
	$[Pt(NH_3)_4](NO_3)_2$		**0.4×10^{-35}**	Y
Pd	$Pd(NO_3)_2$	1.0×10^{-31}, $Pd(OH)_2$	3.9×10^{-6}	X
	$[Pd(NH_2CH_2CH_2NH_2)_2]Cl_2$		**0.2×10^{-31}**	Y
Rh	$RhCl_3$	1.0×10^{-23}, $Rh(OH)_3$	4.8×10^{-6}	X
	$[Rh(NH_3)_5Cl]Cl_2$		2.1×10^{-22}	Z
	$[Rh(NH_2CH_2CH_2NH_2)_3]Cl_3$		**2.5×10^{-51}**	Y
Ir	**$[Ir(NH_3)_5Cl]Cl_2$**	3.3×10^{-64}, $Ir(OH)_3$	–	Y
Re	NH_4ReO_4	–, $Re(OH)_4$	–	X
	$[Re(NH_2CH_2CH_2NH_2)_2O_2]Cl$		–	Y
Ag	$AgNO_3$	2.0×10^{-8}, AgOH	3.1×10^{-5}	X
	$[Ag(NH_2CH_2CH_2NH_2)]NO_3$		**1.8×10^{-8}**	Y

[a] The K_{sp} for a metal hydroxide can essentially indicate whether precipitation will occur under conditions of metal cation and hydroxide ion concentration. If $Q_c < K_{sp}$, unsaturated solution of metal hydroxides, precipitate will not form; If $Q_c > K_{sp}$, supersaturated solution, sudden precipitation may occur when system is disturbed (shock, temperature changes, etc.) [44–46]. K_{sp} for $Re(OH)_4$ was not available in literature because of rearrangement of rhenium hydroxides to rhenium oxo-hydrides [58].

[b] The concentration of hydroxide ions in the LTA zeolite gel is 0.17 mol L^{-1}, and the concentrations of various noble metals are 5.18×10^{-4} mol L^{-1} (Pt), 1.35×10^{-4} mol L^{-1} (Pd), 9.78×10^{-4} mol L^{-1} (Rh), 4.62×10^{-4} mol L^{-1} (Ir), 1.05×10^{-3} mol L^{-1} (Re) and 1.83×10^{-4} mol L^{-1} (Ag). Here, the solubility quotient (Q_c) has the same form as the solubility constant (K_{sp}) expression, but the concentrations of the substances are the free metal cations without bonded ligands (NH_3 or ethylenediamine) and hydroxide ions. The concentrations of metal cations without bonded ligands in metal precursors are calculated based on the stability constants of metal complexes using NH_3 or ethylenediamine as ligands [42,47–50]. No complex stability values of $[Ir(NH_3)_5Cl]Cl_2$, NH_4ReO_4 and $[Re(NH_2CH_2CH_2NH_2)_2O_2]Cl$ have been reported in the literature.

[c] X = Precipitation < 10 s; Y = Clear solution without precipitate > 24 h; Z = Precipitation < 15 min.

units to assemble around these solvated ligand-stabilized precursors via ubiquitous electrostatic and dispersion interactions that typically enforce the self-assembly of zeolite frameworks.

We show here that these methods lead to the selective encapsulation of Pt, Pd, Rh, Ir, Re and Ag clusters within LTA zeolites, which consist of sodalite cages (pore diameter 0.6 nm) and α-cages (pore diameter 1.1 nm). These materials are used to explore the consequences of encapsulation for cluster stability, reactivity and selectivity using reactants of varying sizes and diffusivities. X-ray diffraction (XRD), transmission electron microscopy (TEM) and H_2 or O_2 chemisorption uptakes are used to measure zeolite phase purity, cluster sizes and thermal stability. The oxidative dehydrogenation (ODH) of methanol, ethanol and isobutanol (kinetic diameters: 0.37 nm [16,30], 0.40 nm [31], and 0.55 nm [24,30], respectively) and the hydrogenation (HD) of ethene and isobutene (0.39 nm [32] and 0.50 nm [30], respectively) are used to confirm encapsulation by comparing the reactivity of smaller and larger reactants on metal clusters on LTA and mesoporous SiO_2. Ethene hydrogenation rates with and without thiophene (0.46 nm [11]) also demonstrate the high encapsulation selectivity and the ability of LTA frameworks to protect clusters from contact with organosulfur compounds, thus preserving their surface cleanliness and reactivity during hydrogenation catalysis.

2. Methods

2.1. Materials

Fumed SiO_2 (0.014 μm, 200 ± 25 m^2 g^{-1}, Sigma), $NaAlO_2$ (anhydrous, Riedel-de Haën, technical), NaOH (99.995%, Aldrich), $Pd(NO_3)_2$ (99.99%, Alfa Aesar), $[Pd(NH_3)_4](NO_3)_2$ (10 wt.% in H_2O, Aldrich), $[Pd(NH_2CH_2CH_2NH_2)_2]Cl_2$ (99.9%, Aldrich), $[Pt(NH_3)_4](NO_3)_2$ (99.99%, Alfa Aesar), $[Rh(NH_3)_5Cl]Cl_2$ (Rh 34.5% min, Alfa Aesar), $[Rh(NH_2CH_2CH_2NH_2)_3]Cl_3$ (⩾99.5%, Aldrich), $[Ir(NH_3)_5Cl]Cl_2$ (99.9%, Alfa Aesar), $AgNO_3$ (99.9999%, Aldrich), NH_4ReO_4 (99.9%, Aldrich), $[Re(NH_2CH_2CH_2NH_2)_2O_2]Cl$ (99.8%, Aldrich), $NH_2CH_2CH_2NH_2$ (99.8%, Aldrich), and $NH_3 \cdot H_2O$ (28 wt.% in H_2O, Aldrich).

2.2. Catalyst synthesis

2.2.1. Metal-free LTA

A synthesis gel with the molar composition of 2.6 Na_2O:1.0 Al_2O_3:1.5 SiO_2:92.6 H_2O was prepared. In a typical experiment, 6.0 g $NaAlO_2$ and 4.7 g NaOH were dissolved in 62.0 cm^3 demineralized H_2O and mixed with 3.2 g fumed SiO_2. The resultant gel was transferred into a 500 cm^3 polypropylene container (Nalgene), sealed, and homogenized by magnetic stirring at 800 rpm for 600 s. The gel was stirred in an oil bath at 400 rpm and 333 K for 4 h. After 4 h, the slurry temperature was raised (~0.03 K s^{-1}) to 373 K and the sample was magnetically stirred at 400 rpm for 16 h. The solids were collected on a fritted funnel (Pyrex 36060, 10–15 μm) and washed with deionized water until the rinse liquid reached pH 7–8. The collected sample was treated in ambient air at 373 K for 6 h.

2.2.2. Metal clusters encapsulated within LTA

Pt, Rh and Re clusters encapsulated within LTA. An aluminosilicate gel with the same composition as metal-free LTA synthesis (Table 2) was prepared and magnetically stirred at 400 rpm and 333 K for 3 h. $[Pt(NH_3)_4](NO_3)_2$, $[Rh(NH_2CH_2CH_2NH_2)_3]Cl_3$ or $[Re(NH_2CH_2CH_2NH_2)_2O_2]Cl$ (Table 2) was dissolved in 10.0 cm^3 H_2O and added dropwise to the gel at 0.08 cm^3 s^{-1}. The gel was homogenized by vigorous magnetic stirring (400 rpm) at 333 K for 1 h. Then, the synthesis temperature was raised to crystallization temperature of 373 K (~0.03 K s^{-1}) and the mixture was stirred at 400 rpm for 16 h. The solids were filtered, washed and dried using the same procedure as for metal-free LTA. Samples were treated in air (99.999%, Praxair, 1.67 cm^3 g^{-1} s^{-1}) at 673 K (0.08 K s^{-1}) for 3 h and then in 9% H_2/He (99.999%, Praxair, 1.67 cm^3 g^{-1} s^{-1}) at 623 K (0.08 K s^{-1}) for 4 h to remove the ligands used to stabilize metal precursors and to reduce cations to their respective zero-valent states. Samples were passivated under 0.5% O_2/He (99.999%, Praxair, 1.67 cm^3 g^{-1} s^{-1}) for 1 h at 300 K before air exposure.

Pd, Ir and Ag clusters encapsulated within LTA. The encapsulation of Pd, Ir and Ag clusters within LTA required initially dispersed ligand-stabilized metal precursors over the SiO_2 surface [19,20]. For synthesis of Pd/LTA or Ir/LTA, $[Pd(NH_2CH_2CH_2NH_2)_2]Cl_2$ or $[Ir(NH_3)_5Cl]Cl_2$ (Table 2) was first dissolved in 30.0 cm^3 deionized water and then 3.2 g fumed SiO_2 was added to the mixture. The resulting mixture was stirred at 400 rpm and 333 K for 3 h. Then, 32.0 cm^3 alkaline solution containing 4.7 g NaOH and 6.0 g $NaAlO_2$ was added to the mixture and stirred (400 rpm) at 333 K for 1 h. The temperature was raised to the crystallization temperature of 373 K (~0.03 K s^{-1}) and the slurry was stirred at 400 rpm for 16 h. Ag/LTA was synthesized using ethylenediamine-stabilized Ag precursor, prepared by dissolving $AgNO_3$ in 10.0 cm^3 of 10 wt.% aqueous ethylenediamine solution. Subsequent steps were the same as for the encapsulation of Pd in LTA. The resulting products were separated by filtering, washed and dried using the same procedure as for metal-free LTA. Pd and Ir samples were first treated in air (99.999%, Praxair, 1.67 cm^3 g^{-1} s^{-1}) at 673 K (0.08 K s^{-1}) for 3 h and then in 9% H_2/He (99.999%, Praxair, 1.67 cm^3 g^{-1} s^{-1}) at 623 K (0.08 K s^{-1}) for 4 h to remove ligands and to reduce cations to their respective zero-valent states. The Ag sample was first treated in air (99.999%, Praxair, 1.67 cm^3 g^{-1} s^{-1}) using the same procedure as for Pd/LTA and then in 9% H_2/He (1.67 cm^3 g^{-1} s^{-1}) at 523 K (0.03 K s^{-1}). All samples were passivated under 0.5% O_2/He (99.999%, Praxair, 1.67 cm^3 g^{-1} s^{-1}) for 1 h at 300 K before air exposure.

Silica-supported metal clusters. Metal clusters dispersed on SiO_2 (Davisil®, Grade 646, 300 m^2 g^{-1}, 10 nm mean pore diameter) were prepared by impregnation [24,33] with aqueous solutions of the same metal precursors as in the case of LTA. Solutions (0.1 M) of $[Pt(NH_3)_4](NO_3)_2$, $[Pd(NH_2CH_2CH_2NH_2)_2]Cl_2$, $[Rh(NH_2CH_2CH_2NH_2)_3]Cl_3$, $[Ir(NH_3)_5Cl]Cl_2$, $[Re(NH_2CH_2CH_2NH_2)_2O_2]Cl$ or $[Ag(NH_2CH_2CH_2NH_2)]NO_3$ were prepared and then diluted to 0.004–0.011 M. SiO_2 (5.0 g) was then added to these solutions and the mixture was stirred (400 rpm) for 4 h and subsequently treated at 373 K overnight under rotation to remove water. The solid samples were treated in ambient air at 373 K for 6 h, then heated in air (99.999%, Praxair, 1.67 cm^3 g^{-1} s^{-1}) at 623 K (0.03 K s^{-1}) for 2 h, and in 9% H_2/He (99.999%, Praxair, 1.67 cm^3 g^{-1} s^{-1}) at 623 K (0.03 K s^{-1}) for 2 h. Samples were passivated under 0.5% O_2/He (99.999%, Praxair, 1.67 cm^3 g^{-1} s^{-1}) for 1 h at 300 K before air exposure.

2.3. Characterization

X-ray diffractograms were measured using a Siemens D500 diffractometer and Cu Kα radiation (λ = 0.15418 nm) on samples ground to fine powders and spread uniformly with Vaseline onto a glass slide. Diffractograms were measured for 2θ values of 5–50° at 0.02° intervals. Metal contents were measured by inductively coupled plasma atomic emission spectrometry (ICP-AES) using an IRIS Intrepid spectrometer. Metal dispersions were measured by H_2 chemisorption on Pt, Pd, Rh, Ir and Re samples and by O_2 chemisorption on Ag samples using an Autosorb-1 apparatus (Quantachrome). For H_2 chemisorption, samples were first treated in pure H_2 (99.999%, Praxair; 1 bar) at 623 K (0.08 K s^{-1}) for 1 h and then in dynamic vacuum at 623 K for 1 h. Hydrogen adsorption isotherms were measured at 313 K and 5.0–50 kPa of H_2 for Pt, Rh and Ir samples, and at 623 K and 5.0–50 kPa of H_2 for Re samples [34]. In order to avoid formation of the β-hydride phase in Pd samples [35], isotherms were measured at 343 K and 0.4–1.5 kPa of H_2. For oxygen chemisorption, Ag samples were treated in pure H_2 at 523 K (0.08 K s^{-1}) for 1 h and then evacuated under vacuum at 523 K for 2 h. Oxygen adsorption isotherms were measured at 443 K and 10–30 kPa of O_2 on Ag samples [36]. Metal dispersions were calculated using $H/Pt_s = 1$, $H/Pd_s = 1$, $H/Rh_s = 1$, $H/Ir_s = 2$ [37], $H/Re_s = 4$ [34,38], and $O/Ag_s = 1$ adsorption stoichiometry. Mean cluster sizes were calculated from these dispersion values by assuming spherical clusters [39].

Transmission electron microscopy (TEM) images were taken with a Philips 420 TEM operated at 120 kV. Before TEM analysis, samples were embedded within an adhesive polymer, mechanically thinned, and dimpled and further thinned by ion-polishing at about 3.0 kV on a Gatan PIP. Metal cluster size distributions

Table 2
Initial molar ratios of constituents in synthesis gel of M/LTA samples.

Sample	Metal precursor used	Metal precursor	Na_2O	Al_2O_3	SiO_2	H_2O
Pt/LTA	$[Pt(NH_3)_4](NO_3)_2$	0.048	2.63	1.00	1.46	92.6
Pd/LTA	$[Pd(NH_2CH_2CH_2NH_2)_2]Cl_2$	0.017	2.63	1.00	1.46	125.0
Rh/LTA	$[Rh(NH_2CH_2CH_2NH_2)_3]Cl_3$	0.091	2.63	1.00	1.46	92.6
Ir/LTA	$[Ir(NH_3)_5Cl]Cl_2$	0.043	2.63	1.00	1.46	92.6
Re/LTA	$[Re(NH_2CH_2CH_2NH_2)_2O_2]Cl$	0.098	2.63	1.00	1.46	92.6
Ag/LTA	$[Ag(NH_2CH_2CH_2NH_2)]NO_3$	0.017	2.63	1.00	1.46	92.6

were determined by counting >400 crystallites. The surface area weighted cluster diameters, d_{TEM}, were calculated using $d_{TEM} = \sum n_i d_i^3 / \sum n_i d_i^2$ [39,40].

2.4. Catalytic reactions

All gases [He (99.999%, Praxair), H_2 (99.999%, Praxair), C_2H_4 (5% C_2H_4/He, Praxair, CS), Air (99.999%, Praxair), 20% O_2/He (99.999%, Praxair), 9% H_2/He (99.999%, Praxair), isobutene (99%, Aldrich)] were purified by an O_2/H_2O trap (Agilent) to remove trace H_2O and O_2 (except for O_2/He). CH_3OH (99.9%, Aldrich), C_2H_5OH (99.9%, Aldrich), i-C_4H_9OH (99.9%, Aldrich) were used as received. Thiophene (99%, Aldrich) was purified over degassed molecular sieve 3A and by repeated freeze-vacuum-thaw cycle using dry ice/acetone traps (195 K).

Oxidative dehydrogenation (ODH) and hydrogenation (HD) reactions were carried out in a packed-bed quartz micro-reactor. Catalyst powders were diluted with fumed SiO_2 (Cab-O-Sil, HS-5, 310 $m^2\,g^{-1}$) to a SiO_2/catalyst weight ratio of 10 (100 for Pt/SiO_2). The mixtures were pelletized and sieved to retain aggregates 0.18–0.25 mm in diameter and diluted with quartz granules of similar size to avoid bed temperature gradients. For oxidative dehydrogenation of alkanols, samples were treated in flowing H_2 (1.67 $cm^3\,g^{-1}\,s^{-1}$) at 573 K with 0.08 K s^{-1} (except Ag samples; treated at 523 K with 0.03 K s^{-1}) for 1 h and then cooled to 393 K and treated in 20% O_2/He (1.67 $cm^3\,g^{-1}\,s^{-1}$) for 1 h before catalytic measurements. Alkanol (methanol, ethanol and isobutanol) oxidative dehydrogenation reactions were carried out with 4 kPa alkanol and 9 kPa O_2 at 393 K (353 K for methanol ODH on Pt). Alkene (ethene and isobutene) hydrogenation reactions were carried out with 1.5 kPa alkene and 5 kPa H_2 at 294 K. Ethene hydrogenation reactions with and without 0.1 kPa thiophene were carried out with 1.5 kPa ethene and 5 kPa H_2 at 294 K to probe the ability of LTA structures to protect active sites from thiophene and the extent of encapsulation. Selectivities are reported on a carbon basis as the percentage of the converted alkanol or alkene appearing as a given product. Turnover rates are reported as the number of molecules converted per time normalized by the number of surface metal atoms. Blank experiments using empty reactors, quartz, metal-free Na-LTA, or fumed SiO_2 did not lead to detectable alkanol or alkene conversions at any of the conditions used in this study. Turnover rates did not depend on the extent of dilution for 10:1 and larger diluent: catalyst mass ratios. No deactivation was detected during ODH or hydrogenation reactions on metal clusters on LTA or SiO_2 (over 72 h). Reactant and product concentrations were measured by on-line gas chromatography (Agilent 6890GC) using a methyl-silicone capillary column (HP-1; 50 m × 0.25 mm, 0.25 μm film thickness) and a Porapak Q packed column (80–100 mesh, 1.82 m × 3.2 mm) connected to flame ionization and thermal conductivity detectors, respectively.

3. Results and discussion

We report here the synthesis of noble metal clusters (Pt, Pd, Rh, Ir, Re, and Ag) encapsulated within LTA zeolites by the stabilization of metal precursors using NH_3 or ethylenediamine ligands to prevent their premature precipitation as colloidal oxyhydroxides at the pH and temperatures required for zeolite crystallization. The zeolite framework may function as a ligand, an anion, or a solvent as it assembles building blocks around the metal complexes during nucleation and growth of the zeolite framework [26–29]. The NH_3 and ethylenediamine ligands may act as bridges between metal cations and zeolite frameworks to form stable complexes within cavities that allow adequate volume for these metal complexes [26,27]. These ligands also act as surface functionalization groups for silica and alumina moieties and thus promote the uniform dissemination of metal cationic species throughout the surfaces of mesoporous oxides typically used as catalyst supports [26,41–43].

The precipitation of metal complexes as insoluble oxyhydroxides in aqueous zeolite synthesis media can be prevented by screening of precursors and ligands for their stability. The solubility product constant (K_{sp}) of metal hydroxides ($M(OH)_m$), $K_{sp} = [M^{m+}] \times [OH^-]^m$ ($M^{m+} = Pt^{2+}$, Pd^{2+}, Rh^{3+}, Ir^{3+}, Re^{5+} and Ag^+; $[OH^-] = m\,[M^{m+}]$), is the product of the equilibrium concentrations of the ions in a saturated solution of metal hydroxides, with each concentration raised to an exponent corresponding to the stoichiometric coefficient of that ion in the chemical reaction equation [44–46]. The solubility quotient (Q_c) of metal cations and hydroxide anions, $Q_c = [M^{n+}] \times [OH^-]^n$ ($M^{n+} = Pt^{2+}$, Pd^{2+}, Rh^{3+}, Ir^{3+}, Re^{5+} and Ag^+), is the product of the concentrations of metal cations and hydroxide anions in any solution. Precipitation occurs when Q_c becomes equal to K_{sp}, although slightly higher values may be necessary to overcome nucleation barriers, which require supersaturation of solutions [44–46]. In our synthesis protocols, we maintain the Q_c for metal cations and hydroxide anions at values below K_{sp} for each specific ion pairs (entries in bold, Table 1) to avoid precipitation of metal cations in the zeolite synthesis gels at ambient temperature (~298 K) using suitable ligands to decrease metal cation (Pt^{2+}, Pd^{2+}, Rh^{3+}, Ir^{3+}, Re^{5+} and Ag^+) concentrations through complexation with ligands (Table 1, NH_3 as the ligand: $[Pt(NH_3)_4]^{2+}$ and $[Ir(NH_3)_5Cl]^{2+}$ complex ions; ethylenediamine as the ligand: $[Pd(NH_2CH_2CH_2NH_2)_2]^{2+}$, $[Rh(NH_2CH_2CH_2NH_2)_3]^{3+}$, $[Re(NH_2CH_2CH_2NH_2)_2O_2]^+$ and $[Ag(NH_2CH_2CH_2NH_2)]^+$ complex ions) in aqueous solution [42,44–50].

Precursors were chosen based on their stability and then examined at the pH conditions and temperatures (373 K) required for hydrothermal zeolite syntheses, but in the absence of the silica in order to allow visual detection of any colloids formed (Table 1). Table 1 shows the metal precursors tested for their stability and those shown to remain in solution without precipitation as oxyhydroxides. Preventing premature precipitation provides the opportunity for zeolite building units to self-assemble around ligand-stabilized metal cations during hydrothermal synthesis. These processes are mediated by electrostatic or van der Waals interactions; they are essential for the nucleation and growth of crystalline zeolite frameworks and for the uniform distribution and ultimate encapsulation of active metals within such frameworks [24–29].

3.1. Size and stability of metal clusters

X-ray diffractograms (XRD) of metal-containing LTA zeolites detected crystalline LTA structures after hydrothermal synthesis in the presence or absence of ligand-stabilized metal precursors (Fig. 1 for Pt and Rh; Fig. S1 for Pd, Ir, Re and Ag in LTA). Subsequent thermal treatments in flowing air at 673 K and H_2 at 623 K (Ag at 523 K) for 4 h did not lead to detectable changes in crystallinity. M/LTA (M = Pt, Pd, Rh, Ir, Re, and Ag) samples showed only the characteristic lines of LTA structures, without any detectable diffraction lines for the respective metal phase after treatment in H_2 at 623 K (Ag at 523 K) for 4 h (0.35–1.40 wt.% metal; Table 3). These data confirmed the thermal stability of Na-LTA structures and the substantial absence of large metal crystallites.

Chemisorption uptakes of H_2 or O_2 gave higher dispersions (0.62–0.91, Table 3) for clusters in LTA than on SiO_2 (0.22–0.74, Table 3) at similar metal contents (0.35–1.40 wt.%, Table 3) after treatment in H_2 (99.999%, Praxair) at 623 K (0.08 K s^{-1}) for 1 h and then in dynamic vacuum at 623 K for 1 h. TEM images (Figs. 2 and S2) were used to calculate the dispersity index (DI) of the metal clusters (Fig. 3). The DI value is given by surface-averaged

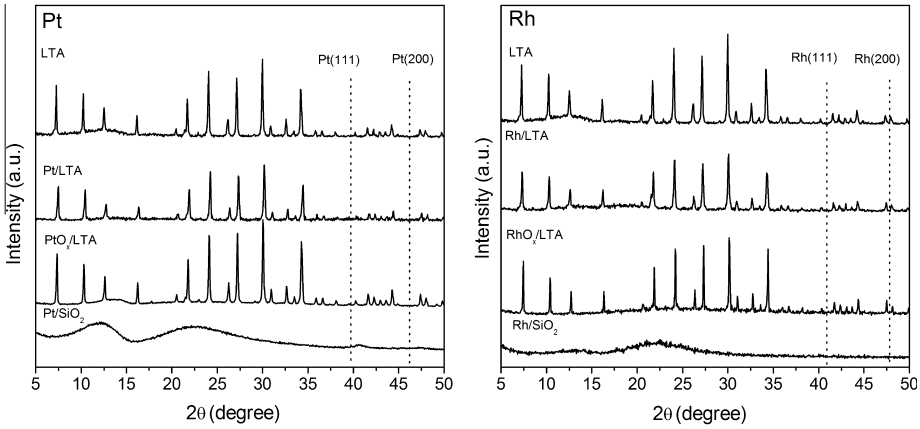

Fig. 1. X-ray diffraction patterns of Pt and Rh containing LTA and SiO_2 samples.

Table 3
Metal content, dispersion, and mean cluster diameter of metal-containing LTA and SiO_2 samples.

Sample	Metal loading (wt.%)[a]	Dispersion[b]	d_{chem}[c] (nm)	d_{TEM}[d] (nm)	Average fraction of α cages of LTA occupied by metal clusters[e] (%)	Average distance between metal clusters within LTA[f] (nm)
Pt/LTA	0.76	0.75	1.5	1.5	0.58	13.2
Pt/SiO_2	0.79	0.61	1.9	2.4	–	–
Pd/LTA	0.58	0.62	1.8	1.9	0.46	14.3
Pd/SiO_2	0.55	0.38	2.9	3.1	–	–
Rh/LTA	0.35	0.89	1.2	1.1	0.91	11.3
Rh/SiO_2	1.10	0.60	1.8	2.1	–	–
Ir/LTA	0.40	0.65	1.5	1.8	0.29	16.7
Ir/SiO_2	1.10	0.74	1.3	1.4	–	–
Re/LTA	0.63	0.78	1.7	1.6	0.35	15.7
Re/SiO_2	0.51	0.22	3.7	4.8	–	–
Ag/LTA	1.40	0.91	1.3	1.4	3.37	7.4
Ag/SiO_2	1.00	0.26	4.5	4.7	–	–

[a] Determined from inductively coupled plasma optical emission spectroscopy.
[b] Metal dispersion (D) estimated from H_2 (for Pt, Pd, Rh, Ir, and Re) or O_2 chemisorption (for Ag) from $D = N_s/N_T$, where N_s is the total number of metal atoms present on the surface and N_T is the total number of metal atoms (surface and bulk).
[c] Mean cluster diameter estimated from the metal dispersion using $d_{chem} = 6 \times \frac{v_m/a_m}{D}$ [39], where v_m is the bulk metal atomic density of Pt (15.10×10^{-3} nm^3), Pd (14.70×10^{-3} nm^3), Rh (13.78×10^{-3} nm^3), Ir (14.24×10^{-3} nm^3), Re (15.06×10^{-3} nm^3) and Ag (17.06×10^{-3} nm^3), and a_m is the surface area occupied by an atom on a polycrystalline surface of Pt (8.07×10^{-2} nm^2), Pd (7.93×10^{-2} nm^2), Rh (7.58×10^{-2} nm^2), Ir (7.73×10^{-2} nm^2), Re (6.60×10^{-2} nm^2) and Ag (8.75×10^{-2} nm^2) [39] metal.
[d] Surface-area-weighted mean cluster diameter (d_{TEM}) estimated from TEM analysis, $d_{TEM} = \sum n_i d_i^3 / \sum n_i d_i^2$ [39], the mean cluster diameter of metal supported on SiO_2 samples is quoted from reference [24].
[e] Average fraction (F) of α cages of LTA occupied by metal clusters calculated from the metal loading (L) and metal cluster diameter (d_{chem}) assuming spherical clusters, $F = \frac{\frac{M \times L}{4/3 \times \pi \times (d_{chem}/2)^3 \times \rho}}{\frac{M \times (1-L)}{M_{LTA}} \times N_A} \times 100\%$, where M is the weight of LTA samples, ρ is the mass density of metal (21.45, 12.02, 12.40, 22.42, 20.53, 10.50 g cm^{-3} for Pt, Pd, Rh, Ir, Re and Ag, respectively [39]), M_{LTA} is the molecular weight (17,520 g mol^{-1}) of the ideal lattice ($[Na_{12}^+(H_2O)_{27}]_8[Al_{12}Si_{12}O_{46}]_8$) of LTA containing one α cage, and N_A is the Avogadro's constant (6.022×10^{23}).
[f] The average distance among metal clusters within LTA calculated from the average fraction (F) of α cages occupied by metal clusters, distance = $2 \times [(1/F) \times a^3]^{1/3}$, where a is the lattice parameter of LTA (1.19 nm) and homogeneous distribution of metal clusters in LTA zeolites was assumed.

diameter ($d_{TEM} = \sum n_i d_i^3 / \sum n_i d_i^2$) divided by the number-averaged diameter ($d_n = \sum n_i d_i / \sum n_i$). This parameter is a measure of the cluster size non-uniformity, with a value of unity corresponding to unimodal clusters and values smaller than 1.5 to relatively uniform size distributions [39,40,51]. The DI value for all M/LTA samples was near unity (1.03–1.12, Fig. 3a), consistent with very narrow size distributions in all samples. The size uniformity and mean cluster diameters evident from these TEM images suggest that metal clusters reside within the LTA crystals, a conclusion confirmed below from catalytic reaction rates for large and small molecules.

Surface-averaged mean cluster diameters (d_{TEM} = 1.1–1.9 nm, Figs. 2 and S2) from TEM images were larger than LTA cages (0.6 nm sodalite cage and 1.1 nm α-cage) for most metals. Metal clusters appear to span more than one cage, but remain isolated from the external surface by many intervening intact cages and windows, thus providing the reactant shape selectivity that we seek (Section 3.2). The formation of crystal defects around growing clusters is expected [3,4], but local lattice defects are difficult to detect by XRD and TEM. Moreover, the formation of metal clusters larger than cage dimensions may occur concurrently with local recrystallization, in a process that would heal any structural defects, thus leading to the observed modestly uniform size and spherical shape of the clusters [52] and making the detection of defects by XRD or TEM impossible.

The use of N-containing ligands as protecting agents in metal precursors can, in some instances, lead to residual fragments strongly bound at metal cluster surfaces, thus making such surfaces inaccessible to molecules in chemisorption and catalytic processes. Surface cleanliness was confirmed by comparing H_2 (for Pt, Pd, Rh, Ir and Re) and O_2 (for Ag) chemisorption uptakes with those expected from the size distribution detected by TEM. A surface cleanliness index (CI) was defined as the ratio of the diameter determined from H_2 and O_2 chemisorption (d_{chem} = 1.2–1.8 nm, Table 3) to the surface-averaged diameter from TEM

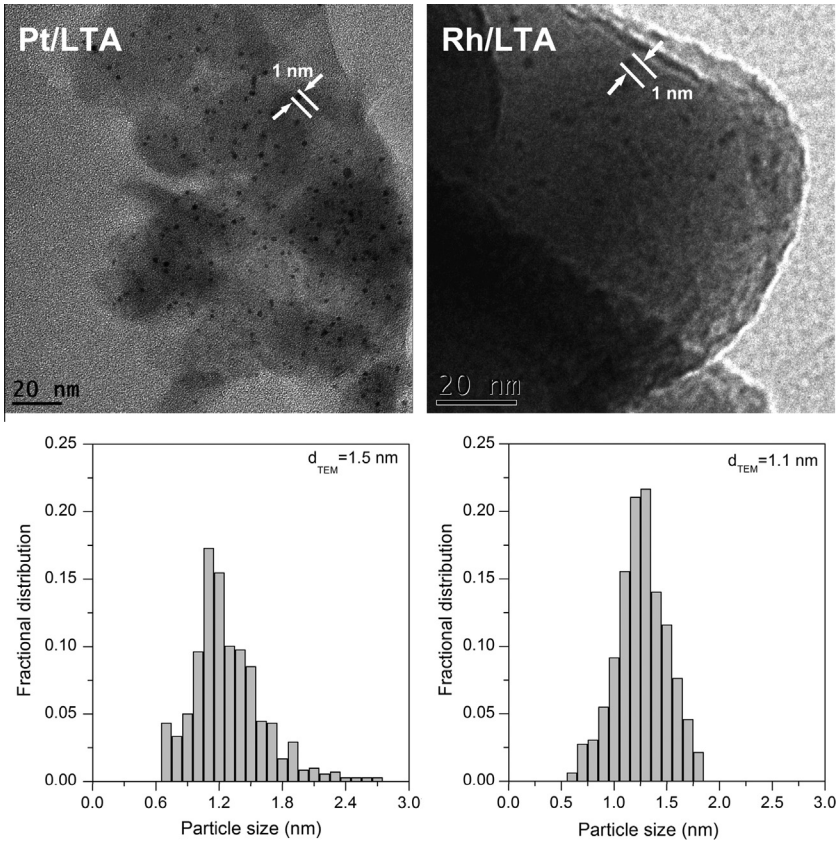

Fig. 2. TEM images and metal cluster size distribution ($d_{TEM} = \sum n_i d_i^3 / \sum n_i d_i^2$) graphs of Pt/LTA and Rh/LTA samples.

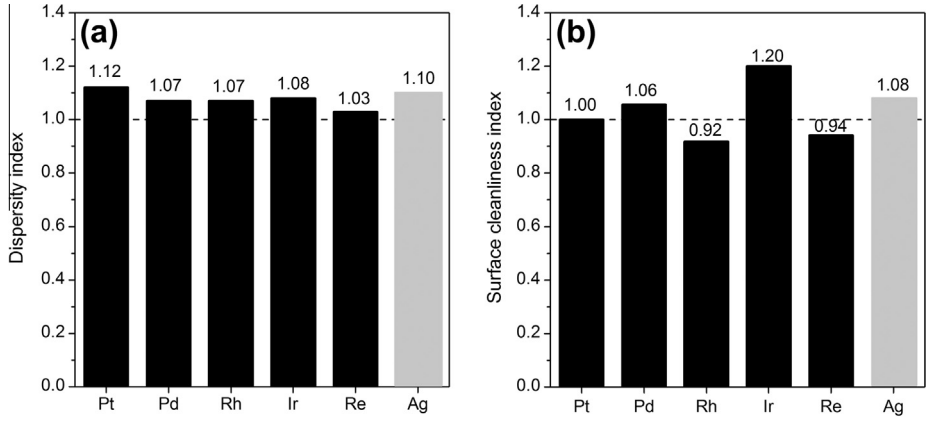

Fig. 3. (a) Dispersity index of metal clusters from TEM characterization and (b) the surface cleanliness index of metal clusters from H_2 (bar in black) or O_2 (bar in gray) chemisorptions and TEM measurements in M/LTA samples (M = Pt, Pd, Rh, Ir, Re and Ag).

images (d_{TEM} = 1.1–1.9 nm, Figs. 2 and S2). A value of unity indicates that clusters detected in micrographs exhibit clean surfaces capable of binding H and O with the expected adsorption stoichiometry after treatment in H_2 at 673 K (Ag at 523 K) for 4 h; values larger than unity would indicate the presence of residues at cluster surfaces. All M/LTA samples gave CI values near unity (0.92–1.20, Fig. 3b), consistent with the presence of essentially clean surfaces and with the complete removal of N-containing ligands or any other residues. Such surfaces are therefore available to catalyze reactions of any molecules that can reach such sites by diffusing through the LTA microporous framework.

Such clean clusters of nearly unimodal size do not sinter or coalesce even at high treatment temperatures (523–873 K), apparently because of their effective isolation by confinement and their spatial uniformity. Only a small fraction (~0.29–3.37%, Table 3) of α-cages in LTA is occupied by clusters and their mean distances are 7.4–16.7 nm (Table 3). The data in Fig. 4 demonstrate this remarkable size stability for the specific case of Pt and Rh and contrast the properties of these metal-containing Na-LTA zeolites with the growth of clusters of similar size dispersed on mesoporous SiO_2.

Pt and Rh mean cluster diameters (d_{chem}) were calculated based on dispersions measured by H_2 chemisorption on Pt/LTA (0.76 wt.% Pt) and Rh/LTA (0.35 wt.% Rh) samples treated in flowing dry air (99.999%, Praxair, 1.67 $cm^3\ g^{-1}\ s^{-1}$) at temperatures between 523 and 873 K for 4 h and then in flowing H_2 (1.67 $cm^3\ g^{-1}\ s^{-1}$) at

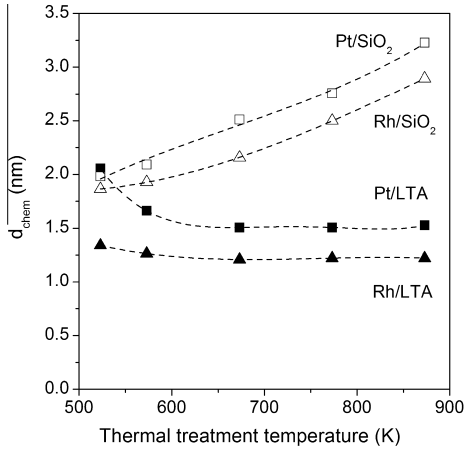

Fig. 4. Effect of air treatment temperature on mean cluster diameter (estimated from the metal dispersion [24,39]) of Pt and Rh containing LTA and SiO_2 samples.

623 K for 4 h. These data are shown together with the corresponding data for Pt/SiO_2 (0.79 wt.% Pt) and Rh/SiO_2 (1.10 wt.% Rh) in Fig. 4. On SiO_2, cluster diameters increased from 2.0 nm to 3.2 nm and 1.9 nm to 2.9 nm for Pt and Rh clusters, respectively, when samples were treated at 523 K and 873 K in flowing dry air (1.67 $cm^3\ g^{-1}\ s^{-1}$) and then in flowing H_2 (1.67 $cm^3\ g^{-1}\ s^{-1}$) at 623 K for 4 h. In contrast, the diameter of Pt and Rh clusters in LTA decreased slightly (from 2.0 nm to 1.5 nm and 1.4 nm to 1.2 nm for Pt and Rh, respectively) when samples were treated from 523 to 673 K in flowing dry air (1.67 $cm^3\ g^{-1}\ s^{-1}$) and then remained constant after treatment in flowing dry air (1.67 $cm^3\ g^{-1}\ s^{-1}$) at temperatures up to 873 K. The initial decrease in cluster diameter reflects either the migration of metal atoms from inaccessible sodalite cages (0.6 nm 6-MR cage, connected by 0.16 nm 4-MR windows) into α-cages (1.1 nm 8-MR cages connected by 0.22 nm 6-MR and 0.41 nm 8-MR windows) [11], where they become accessible to H_2 (0.29 nm kinetic diameter [24]) and O_2 (0.35 nm kinetic diameter [24]) titrants or the more complete removal of ligands or other residues deposited during hydrothermal crystallization [2,3,53,54]. Sodalite cages (0.22 nm window) prevent access and egress of most molecules and make reduction and removal of ligands difficult at low temperatures [11,53,54].

These data, taken together, indicate that confinement of small and uniform metal clusters within LTA voids inhibits coalescence and Ostwald ripening of such metal clusters. Their surfaces are able to bind H and O atoms, suggesting that they can catalyze reactions of any reactants that can diffuse through the windows in LTA zeolites. This protection from cluster coalescence and growth, which occur ubiquitously in mesoporous SiO_2, appears to require that clusters reside within LTA voids. Next, we show that such clusters are indeed located within LTA voids by measuring the rates of reactions of large and small molecules and comparing their reactivities with those measured on mesoporous SiO_2 supports, where reactant size does not influence accessibility and, consequently, reactivity. In doing so, we exploit the intended benefits of encapsulating active sites, present on cluster surfaces within confining zeolite voids, in selecting reactants based on molecular size to demonstrate the ability of our synthetic protocols to achieve encapsulation.

3.2. Reactant selectivity in alkanol dehydrogenation and alkene hydrogenation

Encapsulation confers active sites with the ability to contact only certain reactants and/or to form certain transition states and products based on their molecular sizes and shapes [24,25]. Here, we specifically address reactant shape selectivity by using the oxidative dehydrogenation (ODH) of alkanols (methanol, ethanol and isobutanol; 0.37, 0.40 and 0.55 nm respective kinetic diameters) and the hydrogenation (HD) of alkenes (ethene and isobutene; 0.39 and 0.50 nm respective kinetic diameters); these reactions of large and small molecules allow a quantitative measure of the relative surface areas of Pt, Pd, Rh, Ir, Re and Ag clusters residing within and outside the confined environment of the microporous voids provided by LTA zeolites. The small windows in LTA (0.41 nm × 0.41 nm) allow facile diffusion of methanol, ethanol and ethene reactants, but impede or at least restrict access to intracrystal spaces by larger isobutanol and isobutene reactants. As a result, the relative rates of reactions of small and large reactants on restricted and unrestricted locations provide a measure of the fraction of the metal surface area that resides within LTA voids.

The ratios of ODH or HD turnover rates for small and large reactants, defined as χ ($\chi_{ODH,i} = r_{methanol}/r_{isobutanol}$ or $r_{ethanol}/r_{isobutanol}$, and $\chi_{HD,i} = r_{ethene}/r_{isobutene}$; i = LTA, SiO_2), are larger on clusters encapsulated within LTA than on unconstrained clusters dispersed on mesoporous SiO_2. The ratios of these χ values on LTA and SiO_2 samples can then be used to define an encapsulation selectivity parameter ($\phi = \chi_{j,\ LTA}/\chi_{j,\ SiO2}$, j = ODH, HD) for each reaction–reactant pair [24,25]. This parameter provides an accurate estimate of the extent to which the active surfaces reside within the inaccessible intracrystal regions of LTA, which larger reactants cannot access [24,25]. Encapsulation selectivities (ϕ) near unity would indicate nearly unrestricted access to active sites by both large and small reactants and unsuccessful encapsulation. Large ϕ values, in contrast, provide evidence that clusters predominantly reside within regions that restrict access to the larger reactants, thus making them appear much less reactive than clusters dispersed on accessible mesoporous SiO_2 supports.

3.2.1. Oxidative dehydrogenation (ODH) of alkanols

Alkanol ODH reactions form alkanals as primary products; alkanals undergo secondary reactions with alkanols to form hemiacetals or alkoxyalkanols and then dialkoxylalkanes and carboxylic acids via dehydrogenation or sequential condensation steps [55,56]. Methanol, ethanol, and isobutanol ODH turnover rates ($r_{methanol}$, $r_{ethanol}$ and $r_{isobutanol}$) were measured at low conversions (<5%). These measurements gave the expected high initial selectivities to the corresponding alkanals and much lower selectivities to side products (CO_2 < 9%, Tables 4–7). Small amounts of condensation products (<7%), such as dimethoxymethane, diethoxyethane, and diisobutoxy isobutane also formed. Selectivities to formaldehyde, acetaldehyde, and isobutyraldehyde decreased with increasing reactant conversion (varied using residence time), as expected from their formation as primary products and the secondary reactions that they can undergo.

Methanol ODH turnover rates were slightly higher on SiO_2 than on LTA samples (by factors of 1.0–1.4, Table 4), possibly because of cluster size effects that make smaller clusters in LTA samples (Table 3) less reactive than larger clusters on SiO_2. These size effects reflect the higher binding of chemisorbed oxygen, the most abundant intermediate, on sites of lower coordination, which prevail on smaller clusters [55,57]. Ethanol ODH turnover rates are also slightly higher (by factors of 1.0–2.4, Tables 7) on SiO_2 than on LTA samples; these differences are slightly more pronounced than for methanol, apparently because of slight diffusional constraints for ethanol (0.40 nm kinetic diameter) within LTA crystals [56]. Any effects of cluster size on reactivity would be expected to influence isobutanol ODH reactions similarly, which occur via a similar kinetically relevant step (H-abstraction from adsorbed alkanols or alkoxides by chemisorbed oxygen [54,56]). Yet, isobutanol ODH turnover rates are much smaller on LTA than on SiO_2 samples (~20–160 times; Table 4), thus providing compelling evidence for the selective encapsulation of metal clusters in all LTA samples.

Table 4
Alkanol oxidative dehydrogenation (ODH) and alkene hydrogenation (HD) turnover rates, relative reactivities of small and large reactants and encapsulation selectivity parameters for metal-containing LTA and SiO_2 samples.[a]

Sample	Alkanol ODH reactions				Alkene HD reactions			
	$r_{methanol}$ $\left(mol\left(mol_{surf\text{-}metal}^{-1}\ s^{-1}\right)\right)$	$r_{isobutanol}$ $\left(mol\left(mol_{surf\text{-}metal}^{-1}\ s^{-1}\right)\right)$	$\chi_{ODH,j}$[b] j = LTA, SiO_2	ϕ_{ODH}[c]	r_{ethene} $\left(mol\left(mol_{surf\text{-}metal}^{-1}\ s^{-1}\right)\right)$	$r_{isobutene}$ $\left(mol\left(mol_{surf\text{-}metal}^{-1}\ s^{-1}\right)\right)$	$\chi_{HD,j}$[b] j = LTA, SiO_2	ϕ_{HD}[c]
Pt/LTA	0.53	0.016	32.2	20.1	0.81	0.051	15.8	7.5
Pt/SiO_2	0.56	0.35	1.6		1.30	0.61	2.1	
Pd/LTA	0.45	0.011	40.4	18.4	0.56	0.014	40.0	8.3
Pd/SiO_2	0.51	0.23	2.2		1.60	0.34	4.8	
Rh/LTA	0.025	0.00026	96.2	80.1	0.39	0.0084	46.4	82.9
Rh/SiO_2	0.049	0.042	1.2		0.47	0.84	0.56	
Ir/LTA	0.20	0.011	18.2	14.0				
Ir/SiO_2	0.19	0.15	1.3					
Re/LTA	0.072	0.00084	85.4	19.0				
Re/SiO_2	0.10	0.022	4.5					
Ag/LTA	0.027	0.0024	11.2	13.5				
Ag/SiO_2	0.029	0.035	0.83					

[a] Alkanol oxidative dehydrogenation rates were measured at 4 kPa alkanols and 9 kPa O_2 at 393 K (353 K for methanol ODH on Pt) and alkene hydrogenations at 1.5 kPa alkenes and 5 kPa H_2 at 294 K.
[b] $\chi_{ODH,\ j} = r_{methanol}/r_{isobutanol}$, j = LTA, SiO_2; $\chi_{HD,\ j} = r_{ethene}/r_{isobutene}$, j = LTA, SiO_2.
[c] For ODH reaction, $\phi_{ODH} = \chi_{ODH,\ LTA}/\chi_{ODH,\ SiO2}$; For HD reaction, $\phi_{HD} = \chi_{HD,\ LTA}/\chi_{HD,\ SiO2}$.

Table 5
Methanol ODH turnover rates and selectivities.[a]

Catalyst	Conversion (%)	$r_{methanol}$ $\left(mol\left(mol_{surf\text{-}metal}^{-1}\ s^{-1}\right)\right)$	Product selectivities (%)[b]				
			HCHO (formaldehyde)	MF	DMM	MMOH	CO_2
Pt/LTA	2.7	0.53	80.1	4.5	4.2	2.3	8.9
Pt/SiO_2	2.4	0.56	84.0	7.5	1.4	0.3	6.8
Pd/LTA	3.1	0.45	80.4	11.8	0.1	0.6	7.1
Pd/SiO_2	1.6	0.51	90.2	2.4	0.6	1.7	5.1
Rh/LTA	4.1	0.025	83.1	5.1	0.5	4.2	7.1
Rh/SiO_2	1.8	0.049	93.5	3.2	0.6	0.2	2.5
Ir/LTA	1.8	0.20	91.4	2.9	0.0	3.2	2.5
Ir/SiO_2	2.2	0.19	55.2	30.9	6.2	1.2	6.5
Re/LTA	2.0	0.072	96.9	1.2	0.0	0.0	1.9
Re/SiO_2	1.8	0.10	93.6	2.1	0.3	0.2	3.8
Ag/LTA	2.2	0.027	89.6	5.7	0.4	1.1	3.2
Ag/SiO_2	1.8	0.029	73.4	20.0	0.6	0.0	6.0

[a] Methanol ODH rates were measured at 4 kPa methanol, 9 kPa O_2 and 393 K (353 K on Pt).
[b] MF – methyl formate ($HCOOCH_3$); DMM – dimethoxymethane ($CH_3OCH_2OCH_3$); MMOH – methoxy-methanol (CH_3OCH_2OH).

Table 6
Isobutanol ODH turnover rates and selectivities.[a]

Catalyst	Conversion (%)	$r_{isobutanol}$ $\left(mol\left(mol_{surf\text{-}metal}^{-1}\ s^{-1}\right)\right)$	Product selectivities (%)				
			i-C_3H_7CHO (isobutyraldehyde)	i-C_3H_7COOH (isobutyric acid)	i-$C_3H_7COOC_4H_9$ (isobutyl isobutyrate)	i-$C_3H_7CH_2OC_4H_9OH$ (isobutoxy-isobutanol)	CO_2
Pt/LTA	1.2	0.016	85.7	10.3	0.4	1.1	2.5
Pt/SiO_2	1.4	0.35	77.6	18.3	0.0	1.4	2.7
Pd/LTA	0.7	0.011	91.7	2.9	2.1	0.6	2.7
Pd/SiO_2	1.1	0.23	76.7	15.9	0.6	0.9	5.9
Rh/LTA	0.5	0.00026	95.4	0.1	0.2	2.2	2.1
Rh/SiO_2	1.1	0.042	92.3	0.4	0.4	1.8	5.1
Ir/LTA	1.2	0.16	87.5	1.2	1.2	5.2	4.9
Ir/SiO_2	2.0	0.15	88.8	0.7	0.5	4.1	5.9
Re/LTA	0.1	0.00084	99.7	0.0	0.0	0.3	0.0
Re/SiO_2	0.5	0.022	92.1	0.8	0.3	6.8	0.0
Ag/LTA	1.3	0.0024	95.3	0.1	0.0	1.6	3.0
Ag/SiO_2	2.2	0.035	95.1	0.7	0.1	1.2	2.9

[a] Isobutanol ODH rates were measured at 4 kPa isobutanol, 9 kPa O_2 and 393 K.

These ODH rate measurements give encapsulation selectivities values much larger than unity (13.5–80.1 for methanol and isobutanol ODH (Table 4); 9.9–62.8 for ethanol and isobutanol ODH (Table 7); Fig. 5). These values reflect the much higher $\chi_{ODH,\ LTA}$ values measured on LTA samples (11.2–96.2, for methanol and isobutanol ODH (Table 4); 10.3–69.2, for ethanol and isobutanol (Table 7))

Table 7
Ethanol ODH turnover rates and selectivities.[a]

Catalyst	Conversion (%)	$r_{ethanol}$ $\left(mol\left(mol_{surf\text{-}metal}^{-1}\ s^{-1}\right)\right)$	$\chi_{ODH,j}$[b] j = LTA, SiO_2	ϕ_{ODH}[c]	Product selectivities (%)					
					CH_3CHO (acetaldehyde)	CH_3COOH (acetic acid)	$C_2H_5OC_2H_4OC_2H_5$ (1,2diethoxyethane)	$CH_3COOC_2H_5$ (ethyl acetate)	C_2H_4 (ethene)	CO_2
Pt/LTA	1.4	0.41	17.8	11.1	82.7	4.7	6.9	1.2	1.1	3.4
Pt/SiO_2	1.3	0.55	1.6		81.2	7.2	3.2	2.4	2.1	3.9
Pd/LTA	1.2	0.22	13.8	10.6	87.1	4.1	3.4	0.5	1.2	3.7
Pd/SiO_2	1.0	0.30	1.3		82.5	2.1	5.1	1.5	1.2	7.6
Rh/LTA	2.4	0.018	69.2	62.8	87.2	2.2	2.1	0.7	2.2	5.6
Rh/SiO_2	2.2	0.045	1.1		84.1	2.1	2.0	1.2	2.4	8.2
Ir/LTA	2.0	0.11	12.1	11.0	87.8	1.5	2.6	0.6	1.8	5.7
Ir/SiO_2	2.1	0.16	1.1		84.8	1.4	2.9	1.7	2.2	7.0
Re/LTA	1.1	0.031	35.7	10.5	90.3	2.1	1.9	2.3	1.0	2.4
Re/SiO_2	1.4	0.074	3.4		82.6	3.5	4.4	3.2	1.1	5.2
Ag/LTA	0.8	0.028	10.3	9.9	87.4	2.8	4.2	0.9	2.2	2.5
Ag/SiO_2	1.2	0.032	0.91		85.6	2.1	3.3	4.6	1.2	3.2

[a] Ethanol ODH rates were measured at 4 kPa ethanol, 9 kPa O_2 and 393 K.
[b] $\chi_{ODH,\ j} = r_{ethanol}/r_{isobutanol}$, j = LTA, SiO_2.
[c] $\phi_{ODH} = \chi_{ODH,\ LTA}/\chi_{ODH,\ SiO2}$.

than on SiO_2 samples ($\chi_{ODH,\ SiO2}$ = 0.83–4.5, Table 4). These data, taken together with the size and uniformity of the metal clusters, provide evidence for the tendency of ligand-stabilized precursors to reside within the evolving zeolite structure, as such structures self-assemble during hydrothermal syntheses. These clusters reside predominantly within LTA crystals, where methanol and ethanol, but not isobutanol, can access the catalytic surfaces of metal clusters.

3.2.2. Hydrogenation (HD) of alkenes

Alkene hydrogenation reactions are much less sensitive than alkanol oxidation reactions to cluster size [24,25] and are used here to confirm the conclusions reached based on ODH turnover rates. Alkene hydrogenation led to the exclusive formation of the corresponding alkane on all samples (Table 4). Isobutene cracking products were not detected, indicating that any residual acid sites are unreactive at these conditions. Pt/LTA gave a much higher χ_{HD} values ($\chi_{HD,\ LTA} = r_{ethene}/r_{isobutene}$, $\chi_{HD,\ LTA}$ = 15.8, Table 4) than Pt/SiO_2 ($\chi_{HD,\ SiO2}$ = 2.1, Table 4), consistent with selective encapsulation (ϕ_{HD} = 7.5, Table 4) and with the preferential encapsulation of Pt clusters within LTA voids. Pd/LTA and Rh/LTA also gave encapsulation selectivities (ϕ_{HD}) much larger than unity (8.3 and 82.9 respectively, Table 4 and Fig. 5) confirming that Pd and Rh clusters also reside predominantly within LTA voids accessible only to the smaller ethene reactants. Ethene hydrogenation turnover rates were lower (by a factor of 1.2–2.9, Table 4) on LTA than on SiO_2 samples, apparently because access to metal clusters was restricted by diffusion through LTA apertures or through residual opening around tight-fitting clusters, even for ethene at these low temperatures (294 K) [25].

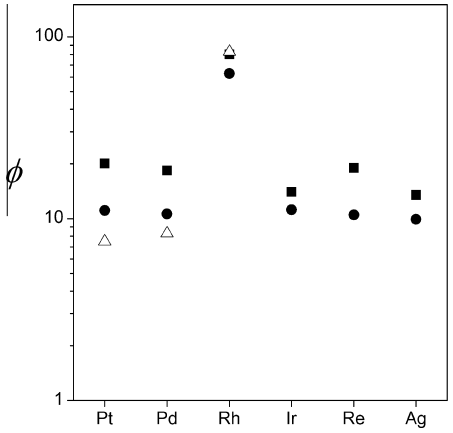

Fig. 5. Encapsulation selectivity parameter (ϕ) [24,25], reflecting the shape selectivity, of various M/LTA samples (M = Pt, Pd, Rh, Ir, Re and Ag) for (i) selective oxidative dehydrogenation (ODH) of methanol and isobutanol (■), ethanol and isobutanol (•) and (ii) selective hydrogenation of ethene and isobutene (△).

These data, taken together with the shape selectivity in alkanol ODH reactions (Fig. 5) and the mean diameter (Table 3), size uniformity (Fig. 3), and stability against coalescence or sintering (Fig. 4), suggest that metal clusters encapsulated within LTA via direct hydrothermal synthesis with ligand-stabilized metal precursors can select reactants based on molecular size and allow access to active sites only by reactants smaller than the interconnecting LTA windows.

3.3. Protection of metal clusters from contact with larger poisons during catalysis

The oxidation and hydrogenation reactions show that LTA selectively sieves molecules based on size and prevents access to metal sites by molecules larger than the connecting LTA windows. Consequently, encapsulated clusters should also resist inhibition or poisoning by large molecules that bind strongly on cluster surfaces (e.g., organosulfur compounds) [16]. In this section, we provide evidence that LTA-encapsulated Pt and Rh clusters can be kept from contact with thiophene (0.46 nm kinetic diameter) [11], a titrant well-known to render metal surfaces unreactive for hydrogenation reactions.

Ethene hydrogenation rates were measured at 294 K on Pt/LTA and Rh/LTA and on the respective SiO_2-supported samples without thiophene and with 0.1 kPa thiophene (Fig. 6). The small windows (0.41 nm × 0.41 nm) in LTA allow the diffusion of ethene and H_2 reactants, but hinder access by thiophene (kinetic diameter 0.46 nm) [11]. As a result, the addition of thiophene (0.1 kPa) to ethene-H_2 reactant mixtures decreased ethene hydrogenation rates to ~0.7 of its values before thiophene addition on LTA-encapsulated Pt and Rh clusters, but fully suppressed rates on both SiO_2-supported samples. This small decrease in hydrogenation rates upon thiophene addition on LTA-encapsulated Pt and Rh clusters reflects diffusional constraints imposed by reversible thiophene physisorption at external LTA surfaces or irreversible thiophene poisoning of metal clusters at unprotected external surfaces. The subsequent removal of thiophene led to the partial recovery of ethene hydrogenation turnover rates in M/LTA (M = Pt and Rh; Fig. 6; to 0.75–0.80 of initial rates), but hydrogenation rates remained

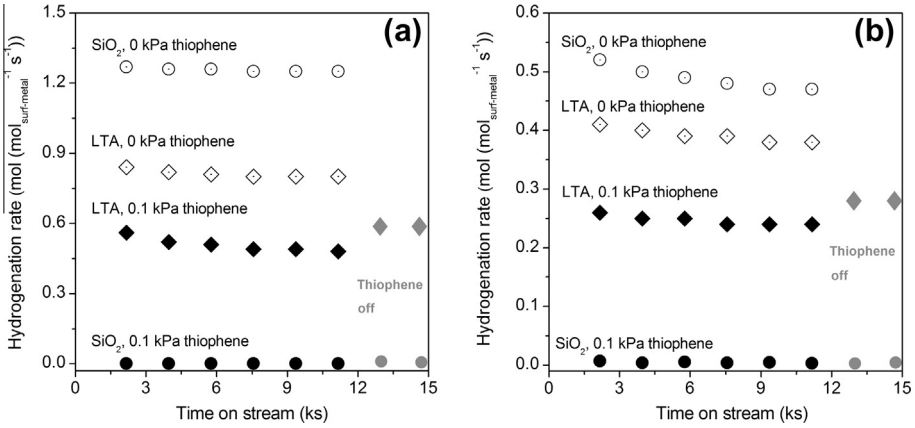

Fig. 6. Ethene hydrogenation rates at 294 K (1.5 kPa ethene) for (a) Pt/LTA and Pt/SiO_2 and (b) Rh/LTA and Rh/SiO_2 samples in the presence (0.1 kPa) and absence of thiophene.

undetectable on SiO_2 samples even after the removal of thiophene. These data show that 0.75–0.80 fraction of the active metal surfaces ($f_{thiophene}$) reside within LTA voids, which are inaccessible to molecules larger than LTA apertures and are thus protected from contact with larger organosulfur compounds.

Encapsulation selectivities determined from alkene hydrogenation reactions (ϕ_{HD}) can also be used to infer the fraction of the measured rates arising from metal clusters residing within LTA voids ($f_{HD} = (\phi_{HD} - 1)/\phi_{HD}$) and to compare such values with those determined from the decrease in ethene hydrogenation upon titration of clusters at external LTA surfaces by thiophene ($f_{thiophene}$). f_{HD} values provide a lower limit for the fraction of the cluster surfaces residing within LTA crystals, where ethene, but not isobutene, can reach active sites. Even ethene, however, shows lower turnover rates on clusters dispersed on LTA than on SiO_2 (Table 4), apparently as a result of diffusional constraints, thus making ϕ_{HD} smaller than in the absence of such diffusional constraints. Therefore, f_{HD} values obtained from encapsulation selectivities are smaller than the actual fraction of active surfaces residing within LTA crystals and represent a lower limit for such values. The values of f_{HD} on Pt/LTA and Rh/LTA are near unity (0.86 and 0.99 respectively), consistent with the nearly complete encapsulation of metal clusters within LTA voids and with $f_{thiophene}$ values (0.75 and 0.80, respectively).

These data and their mechanistic interpretation provide compelling evidence for selective encapsulation and for the general nature of the synthesis protocols reported in this study. The inhibition of premature precipitation of metal precursors and the self-assembly of LTA frameworks around stabilized precursors solvated as cationic species place such precursors, and ultimately the metal clusters derived from them, within confined spaces. As a result, LTA voids stabilize clusters against growth at treatment temperatures that sinter clusters of similar size on mesoporous supports, while also restricting access to active cluster surfaces by larger reactants or poisons.

4. Conclusions

Encapsulation of noble metal clusters (Pt, Pd, Rh, Ir, Re and Ag) within LTA voids was achieved by direct hydrothermal synthesis using ligand-stabilized metal precursors. The synthesis method developed here is based on the selection of appropriate ligands that prevent metal precursor precipitation by forming bulk oxyhydroxides during hydrothermal syntheses, thus allowing their inclusion in the synthesis gel, and promote the assembly of zeolite building units around the solvated ligand-stabilized cationic forms. These materials exhibited high shape selectivities in catalytic oxidative dehydrogenation of alkanols and in hydrogenation of alkenes. They also showed remarkable resistance against poisoning by organosulfur compounds having kinetic diameter larger than zeolite windows and also against thermal sintering because of confinement of metal clusters within zeolite voids. We expect that the present strategy of selective metal encapsulation using ligand-stabilized metal precursors can be extended further to zeolites of different frameworks, void environments and framework compositions and to clusters of other metals, metal oxides and metal sulfides of catalytic importance. These findings hold promise for the design and synthesis of catalysts for hydrotreating molecules in the presence of large heteroatom-containing compounds without poisoning active sites.

Acknowledgments

We thank Dr. Stacey I. Zones (Chevron; University of California at Berkeley) for technical advice and extensive discussions, Dr. George D. Meitzner for the technical review of the manuscript and Chevron Energy Technology Company for the financial support of this research.

Appendix A. Supplementary material

TEM images of LTA-encapsulated metal clusters, dispersions, X-ray diffractograms for metal-containing LTA and their encapsulation selectivities in methanol and isobutanol oxidative dehydrogenation reactions. Supplementary data associated with this article can be found, in the online version, at http://dx.doi.org/10.1016/j.jcat.2013.12.021.

References

[1] W.M.H. Sachtler, Acc. Chem. Res. 26 (1993) 383–387.
[2] P. Gallezot, in: M. Moskovits (Ed.), Metal Cluster, J. Wiley & Sons, 1986, pp. 219–247.
[3] P. Gallezot, in: H.G. Karge, J. Weitkamp (Eds.), Molecular Sieves, Post-Synthesis Modification I, vol. 3, Springer, 2003, pp. 258–298.
[4] W.M.H. Sachtler, Z. Zhang, Adv. Catal. 39 (1993) 129–220.
[5] A. Uzun, B.C. Gates, Angew. Chem. Int. Ed. 47 (2008) 9245–9248.
[6] P.B. Weisz, V.J. Frilette, R.W. Maatman, E.B. Mower, J. Catal. 1 (1962) 307–312.
[7] V.J. Frilette, R.W. Maatman, US Patent 3 373 109, to Mobil Oil Corporation, 1968.
[8] B. Junguin, C. Clement, P. Leprince, R. Montaranl, Bull. Soc. Chim. Fr. 7 (1966) 709–713.
[9] S. Ohgoshi, I. Nakamura, Y. Wakushima, Stud. Surf. Sci. Catal. 77 (1993) 289–292.
[10] J.T. Miller, S.Y. Pei, Appl. Catal. A 168 (1998) 1–7.
[11] H. Yang, H. Chen, J. Chen, O. Omotoso, Z. Ring, J. Catal. 243 (2006) 36–42.
[12] H. Yang, H. Chen, H. Du, R. Hawkins, F. Craig, Z. Ring, O. Omotoso, V. Munoz, R. Mikula, Micropor. Mesopor. Mater. 117 (2009) 33–40.
[13] G.H. Küehl, US Patent 4 191 663, to Mobil Oil Corporation, 1980.

[14] S. Chen, J. Chen, R. Gieleciak, C. Fairbridge, Appl. Catal. A 415–416 (2012) 70–79.
[15] P.A. Jacobs, M. Tielen, J. Martens, J. Mol. Catal. 27 (1984) 11–23.
[16] B.Z. Zhan, E. Iglesia, Angew. Chem. Int. Ed. 46 (2007) 3697–3700.
[17] B.Z. Zhan, M.A. White, T.K. Sham, J.A. Pincock, R.J. Doucet, K.V.R. Rao, K.N. Robertson, T.S. Cameron, J. Am. Chem. Soc. 125 (2003) 2195–2199.
[18] S. Altwasser, R. Gläser, A.S. Lo, P.H. Liu, K.J. Chao, J. Weitkamp, Micropor. Mesopor. Mater. 89 (2006) 109–122.
[19] J.A. Rossin, M.E. Davis, J. Chem. Soc., Chem. Commun. (1986) 234–236.
[20] R.J. Davis, J.A. Rossin, M.E. Davis, J. Catal. 98 (1986) 477–486.
[21] J.C.S. Wu, J.G. Goodwin, M. Davis, J. Catal. 125 (1990) 488–500.
[22] M.E. Davis, G. Saldarriaga, J.A. Rossin, J. Catal. 103 (1987) 520–523.
[23] A.B. Laursen, K.T. Højholt, L.F. Lundegaard, S.B. Simonsen, S. Helveg, F. Schüth, M. Paul, J.D. Grunwaldt, S. Kegnæs, C.H. Christensen, K. Egeblad, Angew. Chem. Int. Ed. 19 (2010) 3504–3507.
[24] M. Choi, Z.J. Wu, E. Iglesia, J. Am. Chem. Soc. 132 (2010) 9129–9137.
[25] S. Goel, Z.J. Wu, S.I. Zones, E. Iglesia, J. Am. Chem. Soc. 134 (2012) 17688–17695.
[26] K.J. Balkus Jr., A.G. Gabrielov, J. Inclusion Phenom. Mol. Recognit. Chem. 21 (1995) 159–184.
[27] K.J. Balkus Jr., C.D. Hargis, S. Kowalai, ACS Symp. Ser. 499 (1992) 347–354.
[28] T.M. Salama, I.O. Ali, A.I. Hanafy, W.M. Al-Meligy, Mater. Chem. Phys. 113 (2009) 159–165.
[29] L.A. Rankel, E.W. Valyocsik, US Patent 4 388 285, to Mobil Oil Corporation, 1983.
[30] Y. Boucheffa, C. Thomazeau, P. Cartraud, P. Magnoux, M. Guisnet, Ind. Eng. Chem. Res. 36 (1997) 3198–3204.
[31] R.L. Van Mao, T.M. Nguyen, G.P. Mclaughlin, Appl. Catal. 48 (1989) 265–277.
[32] R.W. Triebe, F.H. Tezel, K.C. Khulbe, Gas Sep. Purif. 10 (1996) 81–84.
[33] L. Jiao, J.R. Regalbuto, J. Catal. 260 (2008) 329–341.
[34] T. Paryjczak, D. Gebauer, J. Colloid Interface Sci. 72 (1979) 181–190.
[35] P.C. Aben, J. Catal. 10 (1968) 224–229.
[36] T.E. Hoost, R.J. Kudla, K.M. Collins, M.S. Chattha, Appl. Catal. B 13 (1997) 59–67.
[37] G.B. Mcvicker, R.T.K. Baker, R.L. Garten, E.L. Kugler, J. Catal. 65 (1980) 207–220.
[38] D.J.C. Yates, J.H. Sinfelt, J. Catal. 14 (1969) 182–186.
[39] G. Bergeret, P. Gallezot, in: G. Ertl, H. Knozinger, F. Schuth, J. Weitkamp (Eds.), Handbook of Heterogeneous Catalysis, Viley-VCH, 2008, pp. 738–765.
[40] M. Schneider, D.G. Duff, T. Mallat, M. Wildberger, A. Baiker, J. Catal. 147 (1994) 500–514.
[41] L.M. Rossi, I.M. Nangol, N.J.S. Costa, Inorg. Chem. 48 (2009) 4640–4642.
[42] P. Paoletti, Pure Appl. Chem. 56 (1984) 491–522.
[43] H. Zhu, C. Liang, W. Yan, S.H. Overbury, S. Dai, J. Phys. Chem. B 110 (2006) 10842–10848.
[44] S.J. Hawke, J. Chem. Educ. 75 (1998) 1179–1181.
[45] J.G. Speight (Ed.), Lange's Handbook of Chemistry, McGRAW-HILL, 2005, pp. 1.331–1.342.
[46] J. Juodkazyte, B. Sebeka, I. Valsiunas, K. Juodkazis, Electroanalysis 17 (2005) 947–952.
[47] J.E. House (Ed.), Inorganic Chemistry, Elsevier, 2008, pp. 671–685.
[48] C.E. Housecroft, A.G. Sharpe (Eds.), Inorganic Chemistry, Pearson Prentice Hall, 2005, pp. 171–185.
[49] K. Kaas, J. Springborg, Inorg. Chem. 26 (1987) 387–391.
[50] L.H. Skibsted, P.C. Ford, Acta Chem. Scand. A 34 (1980) 109–112.
[51] R.G. Gilbert, M. Hess, A.D. Jenkins, R.G. Jones, P. Kratochvíl, R.F.T. Stepto, Pure Appl. Chem. 81 (2009) 351–353.
[52] N.I. Jaeger, G. Schulz-Ekloff, P. Ryder, Stud. Surf. Sci. Catal. 18 (1984) 299–311.
[53] P. Gallezot, A. Alarcon-Diaz, J.A. Dalmon, A.J. Renouprez, B. Imelik, J. Catal. 39 (1975) 334–349.
[54] P. Gallezot, G. Bergeret, J. Catal. 72 (1981) 294–302.
[55] H.C. Liu, E. Iglesia, J. Phys. Chem. B 109 (2005) 2155–2163.
[56] C. Louis, J.M. Tatibout, M. Che, J. Catal. 109 (1988) 354–366.
[57] J. Lichtenberger, D. Lee, E. Iglesia, Phys. Chem. Chem. Phys. 9 (2007) 4902–4906.
[58] S.K. Tahmassebi, R.R. Conry, J.M. Mayer, J. Am. Chem. Soc. 115 (1993) 7553–7554.